Hindawi Publishing Corporation
International Journal of Antennas and Propagation
Volume 2015, Article ID 504059, 11 pages
http://dx.doi.org/10.1155/2015/504059

Research Article

Experimental Assessment of Linear Sampling and Factorization Methods for Microwave Imaging of Concealed Targets

M. N. Akıncı, T. Çağlayan, S. Özgür, U. Alkaşı, M. Abbak, and M. Çayören

Department of Electronics and Communication Engineering, Istanbul Technical University, 34469 Istanbul, Turkey

Correspondence should be addressed to M. N. Akıncı; akincime@itu.edu.tr and M. Çayören; cayoren@itu.edu.tr

Received 2 February 2015; Revised 27 April 2015; Accepted 13 May 2015

Academic Editor: Lorenzo Crocco

Shape reconstruction methods are particularly well suited for imaging of concealed targets. Yet, these methods are rarely employed in real nondestructive testing applications, since they generally require the electrical parameters of outer object as a priori knowledge. In this regard, we propose an approach to relieve two well known shape reconstruction algorithms, which are the linear sampling and the factorization methods, from the requirement of the a priori knowledge on electrical parameters of the surrounding medium. The idea behind this paper is that if a measurement of the reference medium (a medium which can approximate the material, except the inclusion) can be supplied to these methods, reconstructions with very high qualities can be obtained even when there is no information about the electrical parameters of the surrounding medium. Taking the advantage of this idea, we consider that it is possible to use shape reconstruction methods in buried object detection. To this end, we perform several experiments inside an anechoic chamber to verify the approach against real measurements. Accuracy and stability of the obtained results show that both the linear sampling and the factorization methods can be quite useful for various buried obstacle imaging problems.

1. Introduction

Imaging of concealed targets is an important problem, which can have different applications ranging from medical imaging [1–3] to subsurface sensing [4–9]. Main challenge for such inverse problems is that the solution procedures are expected to capture the electrical parameters (relative dielectric constant ϵ_r, conductivity σ) of whole medium, which includes the buried objects [10–13]. Up to date, many quantitative techniques are developed to obtain the complete electrical parameter distribution of a medium [10, 11]. However, if we take a glance at these formulations, we can see that they involve a considerable computational burden. Being contradictory to quantitative techniques, qualitative inversion methods, which aim to recover only the shape of the scatterers, have relatively simple formulations and require lower computational resources [12, 14]. In contrast to such obvious advantages, qualitative inversion techniques are rarely employed in buried obstacle detection, since these methods have strong a priori knowledge requirements in their original form. In particular, to be able to detect the shape of an inclusion by means of these methods, we must supply these two a priori pieces of information: (i) the dielectric parameters of the surrounding medium and (ii) the scattered field when there is no buried object inside the surrounding medium [12, 14]. It is obvious that fulfilling such strong conditions altogether is of a serious issue in any imaging problem.

There are already several studies to remedy the a priori information problems of qualitative imaging methods [6, 15–21]. In [6], the reciprocity gap-linear sampling method (RG-LSM) is utilized to relieve LSM from the above mentioned constraints. In [15–17, 19], different qualitative methods are assessed in biomedical applications for which a limited a priori information is available. Finally, in [18, 20, 21] LSM is employed in quantitative imaging processes, which can provide an estimate of the dielectric parameters of the whole target.

This paper introduces a practical solution procedure for two famous qualitative inversion schemes, which are the linear sampling method (LSM) [22] and the factorization

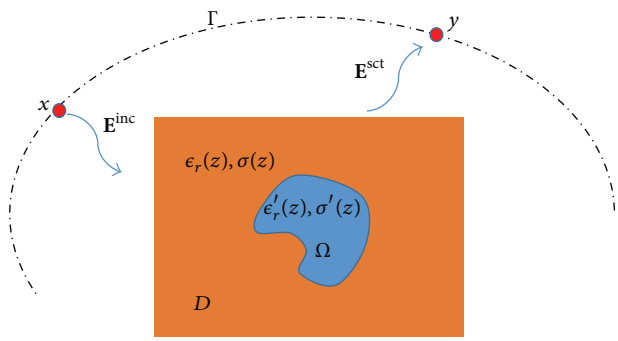

Figure 1: Configuration of the problem (D: the background medium, Ω: the scatterer(s), Γ: the excitation-measurement line, x: the position of the transmitting antenna, y: the position of the receiving antenna, and z: the points inside the sampling domain).

method (FM) [23]. To this end, we propose a strategy to overcome the a priori knowledge requirement on the dielectric parameters of the surrounding medium. Explicitly, we state that it is possible to use LSM and FM in practical situations, whenever the condition (ii) is satisfied. It is important to notice that if (i) is satisfied (ii) is already fulfilled, but the converse is not true. Furthermore, the second condition can be satisfied in certain practical applications like mine sweeping [24, 25], subsurface sensing [4–9] or through-wall imaging [26, 27], and so forth. (For the sake of clarity, let us further explain the through-wall example: it is not easy to completely characterize the dielectric parameters of a wall, but we can easily make a measurement on the different parts of this wall and use one of these measurements as reference.) Consequently, after having the second condition in hand, an accurate shape reconstruction of the inclusion can be obtained by just assuming the outer medium as free space. We prove the effectiveness of the proposed methods with real measurements taken inside an anechoic chamber. Obtained results show that it is possible to localize the buried obstacles whenever we can find a reference medium, which is available to measurement.

In the following section, we briefly revise the LSM and FM, and then, in the subsequent part, we give the formulations of the modified LSM and FM for concealed target detection. Consequently, in the experimental verification section, we will present the results for two different inclusions buried inside dry soil. Throughout the paper, time convention is assumed $\exp(-i\omega t)$ and factored out.

2. Review of Shape Reconstruction Methods

Consider the scenario in Figure 1, where an object Ω, whose relative dielectric permittivity and conductivity are $\epsilon_r'(z)$ and $\sigma'(z)$, is buried into another medium D with electrical parameters of $\epsilon_r(z)$, $\sigma(z)$. The remaining part of the medium is filled with air, which can be modeled as free space. Throughout the paper the wavenumber of any medium is defined as $k = \sqrt{\omega^2\mu\epsilon + i\omega\sigma\mu}$, where ω is the angular frequency of illuminating sources and ϵ, μ are the electrical permittivity, the magnetic permeability of the related medium, respectively. The transmitting and measuring antennas are placed on an arc Γ and we assume that $\Gamma \bigcap \overline{D} = \varnothing$; that is, the measurements are done from outside of the surrounding medium. Here, the measurement arc Γ does not necessarily enclose the object D. The forward scattering mechanism in such a system can be expressed with the well known data and object equations [28]:

$$\mathbf{E}^{\text{sct}}(y) = \int_D \mathbb{G}(y,z)\, O(z)\, \mathbf{E}^{\text{tot}}(z)\, dz; \quad y \in \Gamma,\ z \in D, \tag{1}$$

$$\mathbf{E}^{\text{tot}}(z) = \mathbf{E}^{\text{inc}}(z) + \int_D \mathbb{G}(z,z')\, O(z')\, \mathbf{E}^{\text{tot}}(z')\, dz'; \quad z, z' \in D, \tag{2}$$

where $O(z) = k(z)^2 - k_0^2$ is the so-called object function and $\mathbf{E}^{\text{inc}}$, $\mathbf{E}^{\text{tot}}$, and $\mathbf{E}^{\text{sct}}$ stand for the incident, total, and scattered electric fields, respectively. In (1) and (2), $\mathbb{G}(\cdot,\cdot)$ is the dyadic Green's function of free space, which is defined as [28]

$$\mathbb{G}(z,z') = \left[\mathbb{I} + \frac{1}{k_0^2}\nabla\nabla\right] \frac{e^{ik_0|z-z'|}}{4\pi|z-z'|}, \tag{3}$$

where $\mathbb{I}$ denotes the identity tensor.

2.1. Linear Sampling Method. The general objective of the shape reconstruction methods is to recover an estimate of the support of the inclusion Ω, given the electrical properties of background medium D. Using the electrical properties of the background medium D, the scattered field when there is no object in the reference medium $\mathbf{E}_{\text{ref}}^{\text{sct}}$ can be calculated. Then, the scattered field when there is a scatterer Ω in the reference medium $\mathbf{E}_{\text{all}}^{\text{sct}}$ is measured. Let us assume that Γ is a circle and all antennas are polarized vertically. Then, it is obvious that only vertical component of the scattered electric field $E_{\text{all}}^{v,\text{sct}}$ can be measured. To identify the location of the inclusion, such methods use a common mechanism, which is assigning an indicator function to each sampling point in D [12, 14]. This indicator function exhibits a particular characteristic when the sampling point belongs to inclusion Ω [12, 14]. By plotting the indicator function over all sampling domain

D and searching for the locations at which the particular behavior exists one can reconstruct the shape of the inclusion Ω [12, 14].

Linear sampling method (LSM) is a common example of such support identification methods [22, 29–31]. The main problem that LSM aims to solve is the far field equation [22]. In the above mentioned circular measurement configuration, where N vertical polarized antennas are uniformly distributed on a circle having radius R, the discretized far field equation reduces to

$$\mathbf{F}\mathbf{g} = \widetilde{\mathbf{G}}, \tag{4}$$

where $\mathbf{g} = [g(x_n, z_q)]$; $1 \le n \le N$, $1 \le q \le Q$ is the matrix of coefficients that is to be solved, $\mathbf{F} = [E^{v,\mathrm{sct}}(y_m, x_n)] = [E^{v,\mathrm{sct}}_{\mathrm{all}}(y_m, x_n)] - [E^{v,\mathrm{sct}}_{\mathrm{ref}}(y_m, x_n)]$; $1 \le m, n \le N$ stands for the discretized far field operator, whose elements are the vertical component of the scattered electric field measured by mth antenna when nth antenna acts as source. In (4), $\widetilde{\mathbf{G}} = [\widetilde{G}^{vv}(y_m, z_q)]$; $1 \le m \le N$, $1 \le q \le Q$ is the vertical component of the electrical field measured at point $z_q \in D$, $1 \le q \le Q$ when a vertically polarized infinite small dipole, which is located at the position of mth receiving antenna, illuminates the reference medium. LSM states that the solutions of (4) is finite only if the sampling point $z_q \in D$, $1 \le q \le Q$ coincides with a scatterer Ω. It is important to note that (4) is severely ill posed and a regularization scheme must be utilized to obtain a stable solution [22]. Here, we can utilize from the Tikhonov regularization

$$\mathbf{g} = \left(\mathbf{F}^*\mathbf{F} + \alpha\mathbf{I}\right)^{-1}\left(\mathbf{F}^*\widetilde{\mathbf{G}}\right), \tag{5}$$

where $(\cdot)^*$ stands for the conjugate transpose operator. Here, the regularization parameter α is determined by imposing the following condition:

$$\frac{\sigma_N}{\alpha^2 + \sigma_N^2}\frac{\sum_{q=1}^{Q}\left|\left\langle \widetilde{G}^{vv}\left(\cdot, z_q\right), u_N(\cdot)\right\rangle\right|}{Q} = \frac{1}{\sigma_1}\max_{1\le q\le Q}\left|\left\langle \widetilde{G}^{vv}\left(\cdot, z_q\right), u_1(\cdot)\right\rangle\right|, \tag{6}$$

where $\langle\cdot,\cdot\rangle$ denotes the inner product on receiving points and $\Sigma = \{\sigma_1, \sigma_2, \ldots, \sigma_N\}$; $U = \{u_1, u_2, \ldots, u_N\}$ stand for the singular values, the left singular vectors of $\mathbf{F}$, respectively [32]. Hence, the indicator function for LSM is defined as the reciprocal of norm of the solutions of (4) [22], which can be given as

$$I\left(z_q\right) := \left(\sum_{n=1}^{N}\left|g\left(x_n, z_q\right)\right|^2\right)^{-1}; \quad 1 \le q \le Q. \tag{7}$$

By plotting I on the entire sampling domain, an illustration of the shape of the inclusion Ω can be recovered. For a more detailed investigation of the theoretical framework of the LSM, the reader is proposed to see [22, 29].

2.2. Factorization Method. Another famous support identification algorithm is the factorization method (FM), which is developed as an alternative to LSM [23, 33, 34]. The purpose of FM is to investigate the solvability of the following matrix equation [23]:

$$\left(\mathbf{F}^*\mathbf{F}\right)^{1/4}\mathbf{g} = \widetilde{\mathbf{G}}, \tag{8}$$

where $\mathbf{F}$ and $\widetilde{\mathbf{G}}$ stand for the far field operator and the matrix of Green's functions defined in (4). The equation in (8) has finite solutions if and only if the sampling point $z_q \in D$, $1 \le q \le Q$ coincides with an object Ω [23]. In [23], it is shown that the above equation has finite solutions if and only if

$$I\left(z_q\right) := \left[\sum_{m=1}^{M}\frac{\left|\left\langle \widetilde{G}^{vv}\left(\cdot, z_q\right), \psi_m(\cdot)\right\rangle\right|^2}{\left|\lambda_m\right|}\right]^{-1}; \quad 1 \le q \le Q,\ M \le N \tag{9}$$

is greater than 0. Here, $\Psi = \{\psi_1, \psi_2, \ldots, \psi_N\}$ and $\Lambda = \{\lambda_1, \lambda_2, \ldots, \lambda_N\}$ are the sets of eigenfunctions-eigenvalues of the far field operator $\mathbf{F}$, respectively. Note that the regularization for (9) can be done by a spectral cut-off of the eigensystem of $\mathbf{F}$ at $m = M \le N$. Similar to the LSM, a plot of I on the sampling domain D gives an estimate of the support of the inclusion. More detailed mathematical discussions regarding FM can be found in [23, 33, 34].

3. Solution to Imaging of Buried Objects

Although the above procedures are simple to implement and stable in nature, they are rarely employed in experimental concealed target detection. This is basically due to the fact that they require some a priori information, which cannot be available in most of the practical problems. Those requirements in the above scenarios can be stated as follows.

(i) Far field equation in (4) requires one to know the dyadic Green's function $\widetilde{\mathbf{G}}$, which is directly connected with the electrical parameters of the surrounding medium (i.e., $\epsilon_r(z)$, $\sigma(z)$ in Figure 1).

(ii) Furthermore, to be able to construct the equation system in (4) the scattered field due to inclusion, that is, $E^{v,\mathrm{sct}}$ in (4), must be known. Therefore, we must compute (or at least approximate) $E^{v,\mathrm{sct}}_{\mathrm{ref}}$, which is the scattered field from the reference medium D.

It is very important to distinguish between these two conditions. First of all, satisfying the first condition, which states that one must have dyadic Green's function $\widetilde{\mathbf{G}}$, seems to be unrealistic in many microwave measurement systems. However, the second condition can be satisfied in certain imaging problems for which an extra measurement of a reference medium is feasible [4–9, 24–27]. As an example, in through-wall imaging or subsurface sensing problems, it is not hard to find a reference medium available to measurement, but measuring such a reference does not provide us a model for the distribution of the electrical parameters of

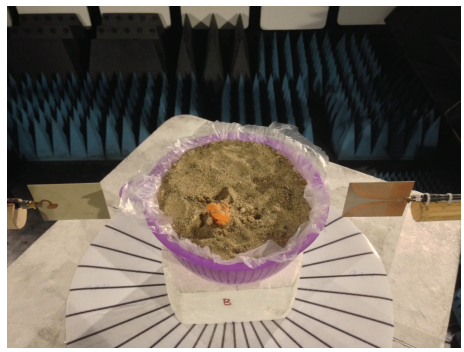

Figure 2: Measurement setup.

the surrounding medium D. Let us think of such cases in which we have a reference medium available to measurement, and then we propose that the far field equation in (4) can be modified as

$$\mathbf{F}\mathbf{g} = \mathbf{G}, \tag{10}$$

where Green's function of free space $\mathbf{G}$ is replaced with Green's function of the background medium $\widetilde{\mathbf{G}}$. The dyadic Green's operator $\mathbf{G}$ can be computed by (3); therefore, by solving the modified equation in (10) via Tikhonov regularization defined in (5), (6) and by plotting the indicator function I as in (7), an estimate of the support of the inclusion Ω can be obtained.

Similarly, the main equation of FM can be changed as

$$\left(\mathbf{F}^{*}\mathbf{F}\right)^{1/4}\mathbf{g} = \mathbf{G}. \tag{11}$$

Hence, the indicator function I for FM can be obtained in a similar manner to (9). Although there are different approaches for an optimal regularization of the FM [35, 36], we set $M = N$ by relying on our numerical observations. Consequently, a plot of I over the entire sampling domain D provides a reconstruction of the shape of the buried targets.

4. Experimental Verification

In the light of the theoretical evaluations, this section includes the discussions of what kind of results can be obtained for different scatterers and for what applications the approach that we have proposed can be useful. To illustrate the applicability of the methodologies, we prepare the measurement setup shown in Figure 2. The system consists of computer controlled turn table, a vector network analyzer (VNA, Agilent N5230A), and two vertically polarized Vivaldi antennas, which are examples of classical ultrawideband antennas [37–40]. Calibration between VNA and the antennas is done by means of the Agilent N4691B electronic calibration module. For all cases, the reference medium is dry soil. S-parameters are sampled at 24 points when the scatterer is chosen as water and 12 points when the scatterer is air. (The number of measurements is selected according to the number of degrees of freedom of the scattering problem. Note that the radii of the targets are smaller than one wavelength (wavelength in free-space) even for the highest frequency. Hence $2k_0a \approx 12$ measurements are sufficient in general. To guarantee a better reconstruction quality for the water filled target, we increase the number of measurements to 24 [41].) Unless otherwise stated, the measurement points are uniformly distributed on the circle having a radius of 17 cm. For the conversion between S-parameters and electric field, the method proposed in [42] is employed. Basically, using a canonical target, a single coefficient for each frequency f, is calculated as

$$C(f) = \frac{\sum_x \sum_y E_{\text{sim}}(x, y, f)\, S^{*}_{\text{meas}}(x, y, f)}{\sum_x \sum_y \left|S_{\text{meas}}(x, y, f)\right|^2}, \tag{12}$$

where $E_{\text{sim}}(x, y)$ denotes the vertical component of simulated scattered field and $S_{\text{meas}}(x, y)$ stands for the measured scattered S-parameter for the same polarization. In (12), the transmitter is located at x, whereas the position of the receiver is given by y. After calculating the conversion coefficients $C(f)$, the vertical component of the scattered electrical field for any target can be given as

$$E_{\text{meas}}(x, y, f) = C(f)\, S_{\text{meas}}(x, y, f). \tag{13}$$

In our measurement configuration, the calibration target is selected as a metallic cylinder with a radius of 10 cm and its simulated field is computed analytically [43]. As given in Figure 3, calibrated electric field of the cylinder and the analytical solution have a good agreement. To increase the frequency diversity of the measurement, S-parameters are sampled at 41 frequencies equilinearly distributed on 2 GHz–6 GHz interval. Multifrequency reconstructions are obtained by summing all single frequency indicators and normalizing the final values with respect to their maximum value [44]. To be able to make pointwise summations on single frequency reconstructions, the sampling domain is discretized into 40×40 points for all frequencies. As a final note, it must be emphasized that this measurement setup can only produce 2D slice images, since the antennas do not sweep along vertical axis [32]. Therefore, all reconstructions given here is for the horizontal slice going through the midpoints of the antennas. (Although we stress that the algorithms produce 2D

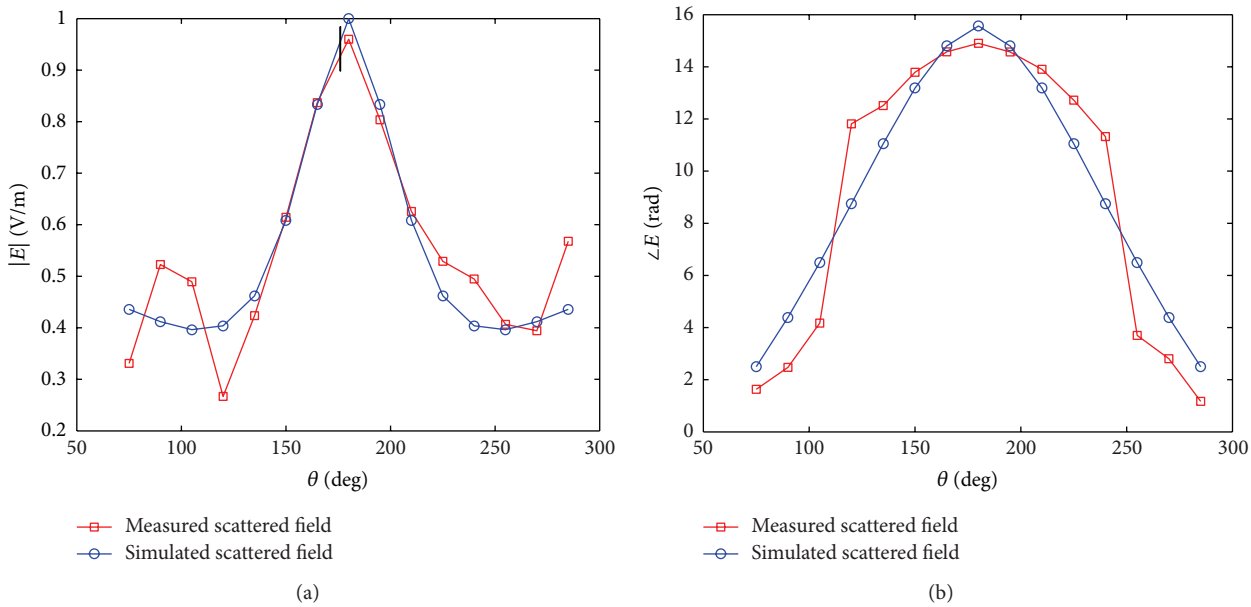

Figure 3: Measured (red squares) and simulated (blue circles) electric fields for canonical target at 4 GHz: (a) normalized absolute values (b) phase.

images, full 3D modeling is employed for all configurations. Explicitly, the equations given in (10), (11) are solved without simplifying the operators to 2D case. The only modification is that (10) and (11) are solved for only those points, which belong to the horizontal slice that is going through the midpoints of the antennas.)

The first material, for which the measurements are performed, is shown in Figure 4(a). In this case, two measurements are performed. First the dry soil is measured, and,then for the second measurement, a water filled balloon with a radius of 3 cm is buried into soil. The center of the balloon is located at ($u = -1$ cm, $v = 3$ cm). Here, we adopt the following axis definitions: v axis is parallel to ruler in Figures 4(a) and 5(a) and its positive end is directed towards right side, u is the axis, which can be obtained by rotating v at an amount of 90° in the counter clockwise direction. Obtained results for LSM and FM are given in Figures 4(b) and 4(c), respectively. Obviously, both methods recover the horizontal profile correctly without using any a priori knowledge on the electrical properties of the dry soil. An important point that must be mentioned is that both algorithms reconstruct the support of the midslice of the inclusion, although the antennas are not aligned with the midslice of the scatterer. By referring to our empirical observations, we can say that these methods exhibit this peculiar behavior in general. Another interesting point is the quality of the reconstructions for these two methods are very close to each other. This in fact is expected since these methods originate from similar mathematical principles.

After demonstrating the applicability of the proposed approach, we investigate how the information of the exact Green's function affects the quality of the results. For this aim, the dyadic Green's function of the reference medium is computed with a 3D Method of Moments solver, utilized from biconjugate gradient fast Fourier transform method [45]. Here, the relative dielectric permittivity and conductivity of the dry soil is taken as $\epsilon_r = 3.5$ and $\sigma = 0.05$ S/m for all frequencies of illumination [46, 47]. The results with the exact Green's function are given in Figures 4(d) and 4(e) for LSM and FM, respectively. As can be seen the reconstructions of proposed formulations are very similar to Figures 4(d) and 4(e). Hence, it can be concluded that, with the proposed method, unavailability of the exact dyadic Green's function does not cause a significant quality degradation.

Next, we continue with a second example to further illustrate the performance when the scatterer is weak (i.e., the electrical properties of the buried material is low.) and the electrical contrast between the inclusion and the surrounding medium is low. (Note that the electrical properties of the water is $\epsilon_r = 75$ and $\sigma = 2$ S/m at 3 GHz [48].) To this end, the material shown in Figure 5(a) is prepared. For this case, an air filled balloon is buried into dry soil. The coordinates of the center of the balloon are measured as ($u = 6$ cm, $v = 1$ cm) and the radius of the scatterer is 2 cm. Reconstructions for LSM and FM are shown in Figures 5(b) and 5(c), respectively. As it can be observed from the results, the proposed formulations produce an estimate of the shape of the inclusion even when the scatterer is weaker in electrical contrast.

Up to now, we show the feasibility of the presented method when the measurements are taken on a full aperture. However, the common measurement schemes for concealed target detection problems consist of a limited incidence-observation angles. Thus, to be able to give a merit to the presented formulations, they must be analyzed when such a measurement configuration is employed. For this aim,

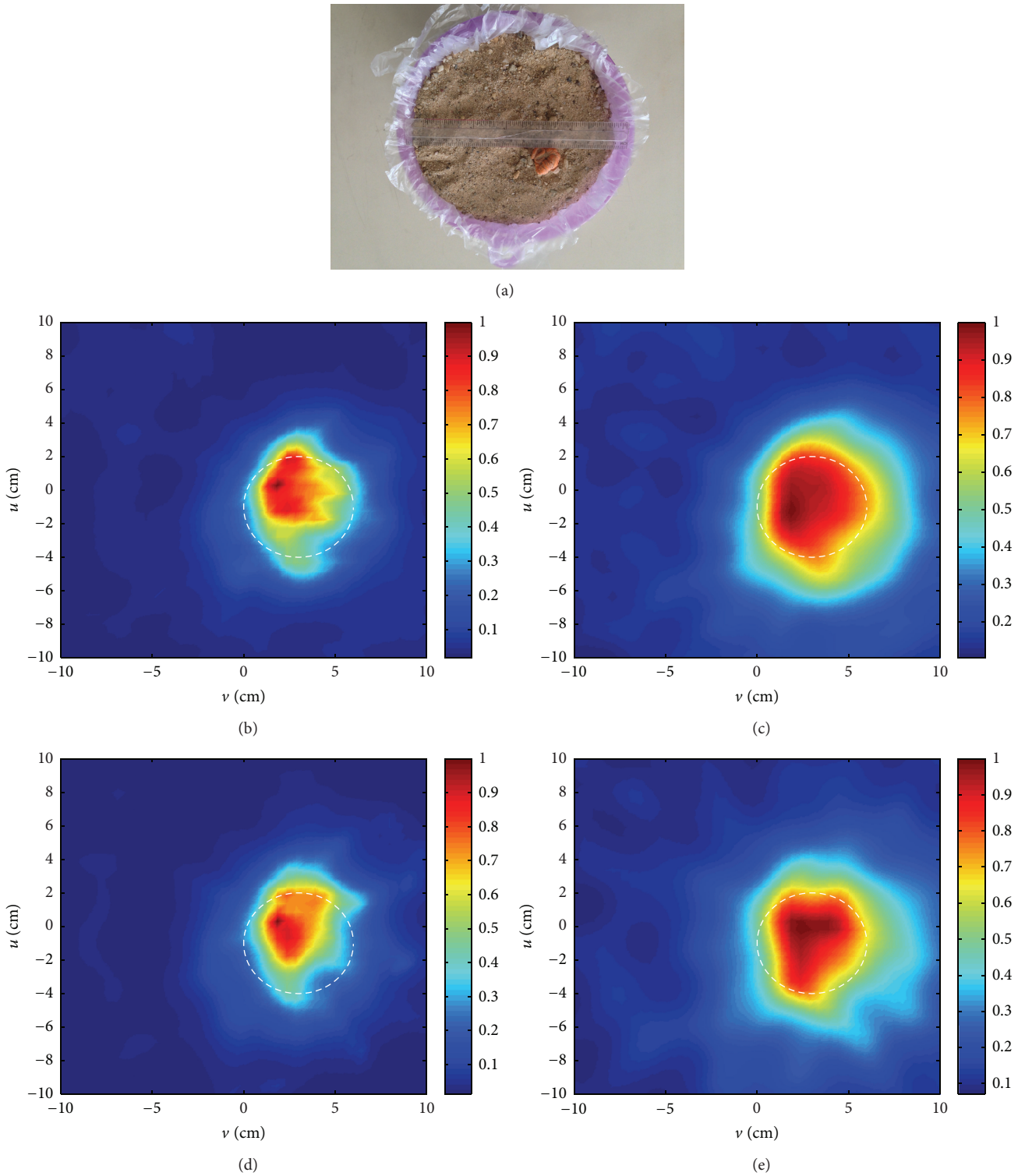

Figure 4: (a) Measured material, (b) LSM reconstruction with the proposed formulation, (c) FM reconstruction with the proposed formulation, (d) LSM reconstruction with the exact Green's function, and (e) FM reconstruction with the exact Green's function, for the scatterer filled with water.

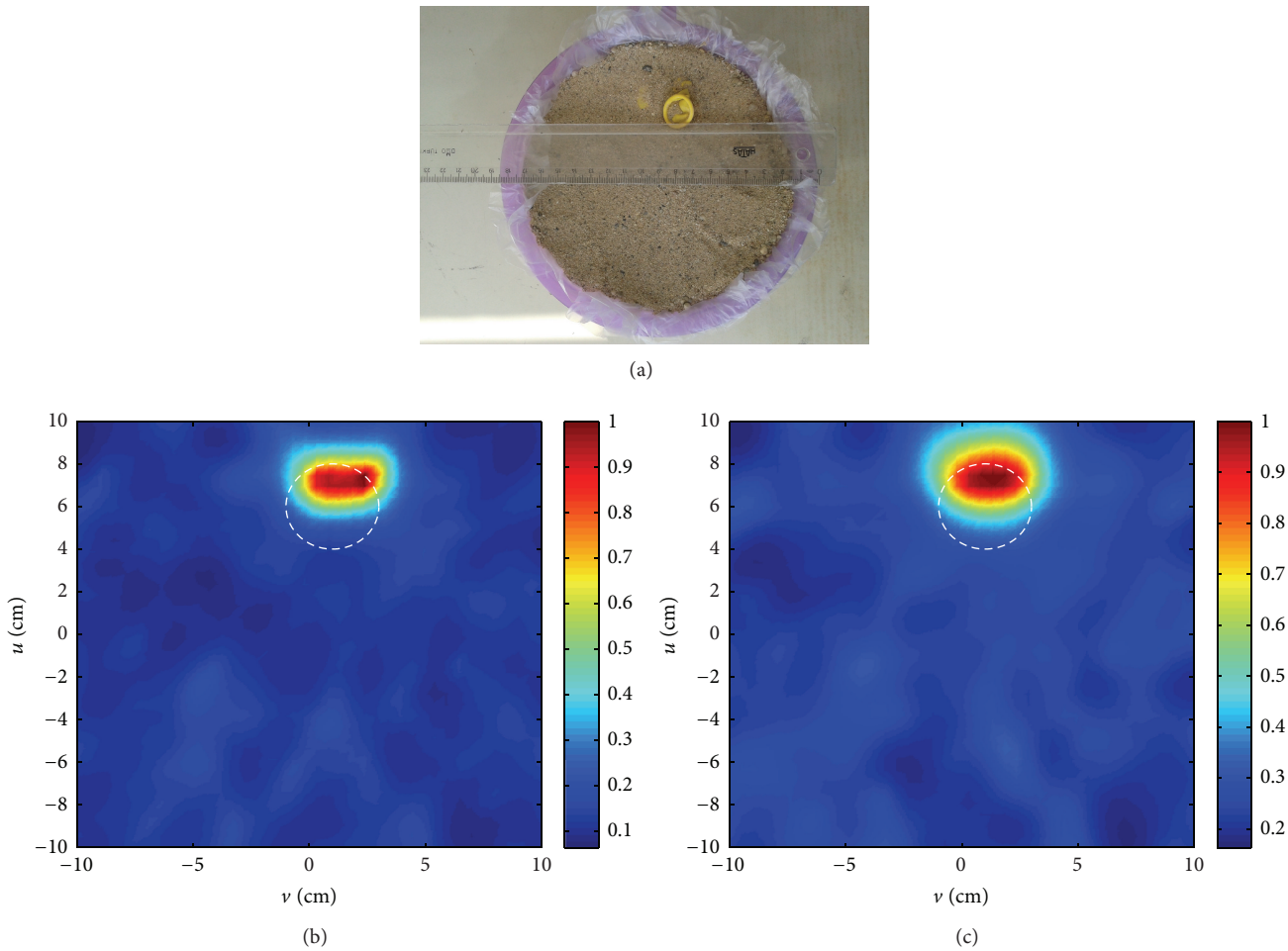

Figure 5: (a) Measured material, (b) LSM reconstruction, and (c) FM reconstruction for the scatterer filled with air.

certain parts of the obtained scattering matrix are cut and the inversions are applied by using only these measurements. The imaging results when the scatterer is water filled balloon are given in Figure 6. Here, for Figures 6(a) and 6(b), the transmitting and measuring antennas are located on the same arc, which is defined as $90^\circ < \theta < 270^\circ$, $r = 17$ cm. Such a measurement scheme is mostly employed in subsurface sensing [4–9] and through-wall imaging problems [26, 27]. As can be seen from the results, the quality of the reconstructions decreases for both LSM and FM, when compared with the previous results. Nevertheless, both methods can provide some clues about the shape of the scatterers. Another typical measurement configuration is the one in which the transmitting and receiving antennas are located on different arcs. Here, the union of these two arcs can enclose the material under test. Such a configuration may be useful in nondestructive testing problems [49–51]. The results for this type of measurement scenario are given in Figures 6(c) and 6(d) for LSM, FM, respectively. For these results, the scatterer is the water filled balloon as in Figures 6(a) and 6(b). As can be observed from these images, this kind of measurement produces better reconstructions than the results in Figures 6(a) and 6(b). This phenomenon can be simply explained as the increase in the union of the measurement-excitation apertures leads to better results.

Finally, the same measurement configurations can be applied to the air filled scatterer. The obtained results, when the transmitting and receiving antennas are located on the same arc, are given in Figures 7(a) and 7(b) for LSM, FM, respectively. It is obvious that both algorithms are also capable of providing an estimate of the shape of the air filled scatterer. Another point that must be stressed is that the reconstruction for LSM is more clear than the one for FM. In fact, there can be many factors which can cause such performance differences. A few of them can be stated as selection of regularization parameter for LSM, the number of eigenvalues taken into account for FM and, and so forth. As for the two last examples for the weak scattering target, the case in which the transmitting and receiving antennas are located on different arcs is considered. The obtained reconstructions for LSM and FM are given in Figures 7(c) and 7(d), respectively. By observing the results, it can be inferred that both methods can give an estimate of the shape and the location of the scatterer. Similar to the results in

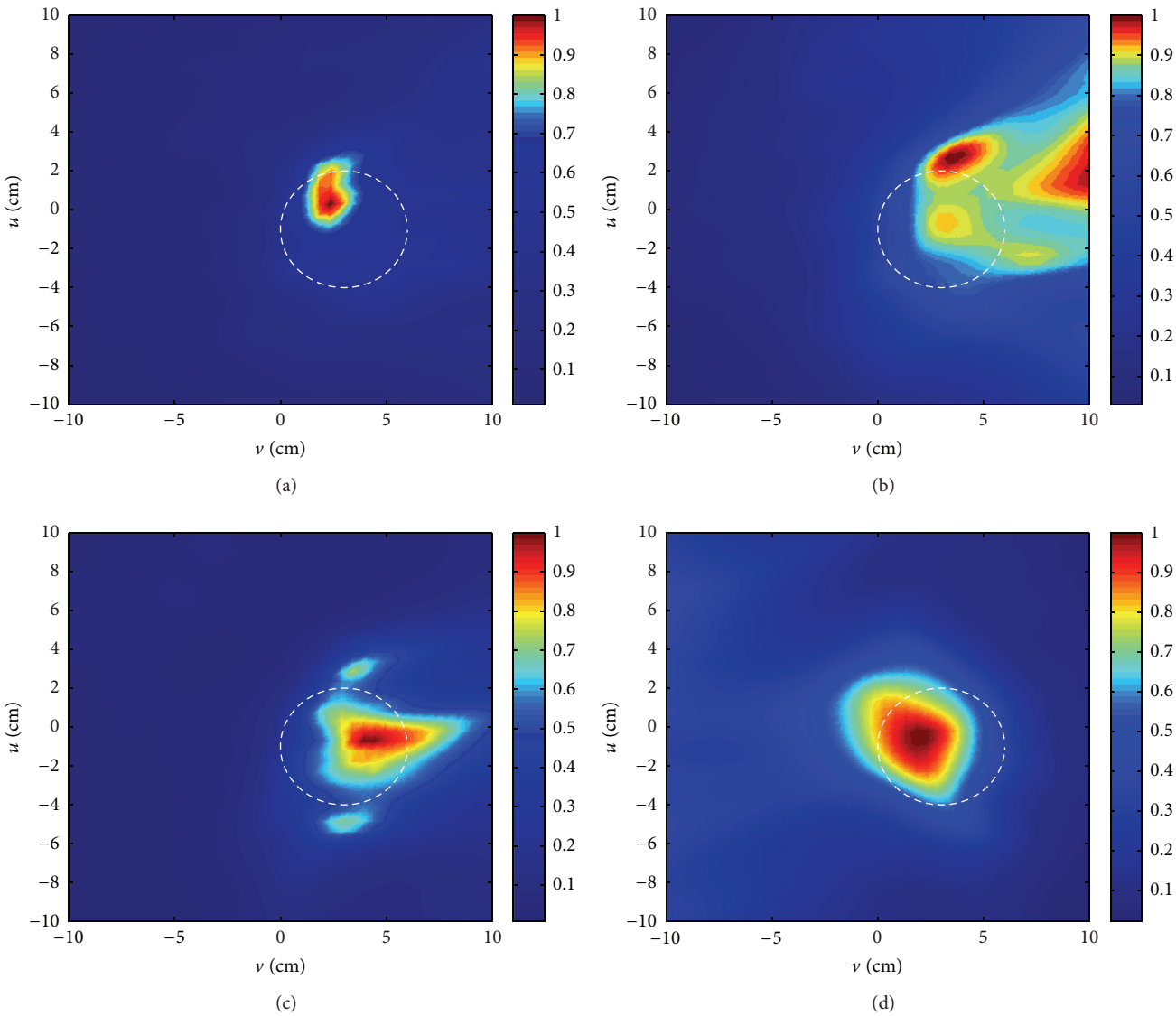

Figure 6: Reconstructions obtained for the water filled scatterer by using (a) LSM, (b) FM when the transmitting and receiving antennas are located on $90^\circ < \theta < 270^\circ$, $r = 17$ cm, and (c) LSM, (d) FM when the transmitting and receiving antennas are located on $90^\circ < \theta < 270^\circ$, $r = 17$ cm, and $-90^\circ < \theta < 90^\circ$, $r = 17$ cm, respectively. (Here $\theta = \tan^{-1}(u/v)$ and $r = \sqrt{u^2 + v^2}$.)

Figures 7(a) and 7(b), LSM gives a more clear estimate compared to the FM. This performance difference can be explained by using the same arguments stressed in the above. Consequently, we can conclude that the modified formulations can be employed in such real measurement scenarios to obtain an estimate of the shape and the location of the buried obstacles.

5. Conclusions and Future Work

In this paper, we propose an experimental technique to move around the a priori information requirements of the qualitative methods. The proposed approach works for the situations where an extra measurement for the reference medium is feasible. In particular, we modified the formulations of two well known qualitative methods, the linear sampling method (LSM) and the factorization method (FM). The accuracy of the modified formulations is tested against realistic measurements. Besides showing the accuracy of the presented formulations, the obtained results imply the feasibility of proposed approach, especially for subsurface imaging, where the targets are buried into soil.

Lastly, we want to emphasize that the proposed formulations are important from the aspect that it can make the usage of qualitative methods possible in many real world problems. Future research will be devoted to application of these methods in more realistic environments.

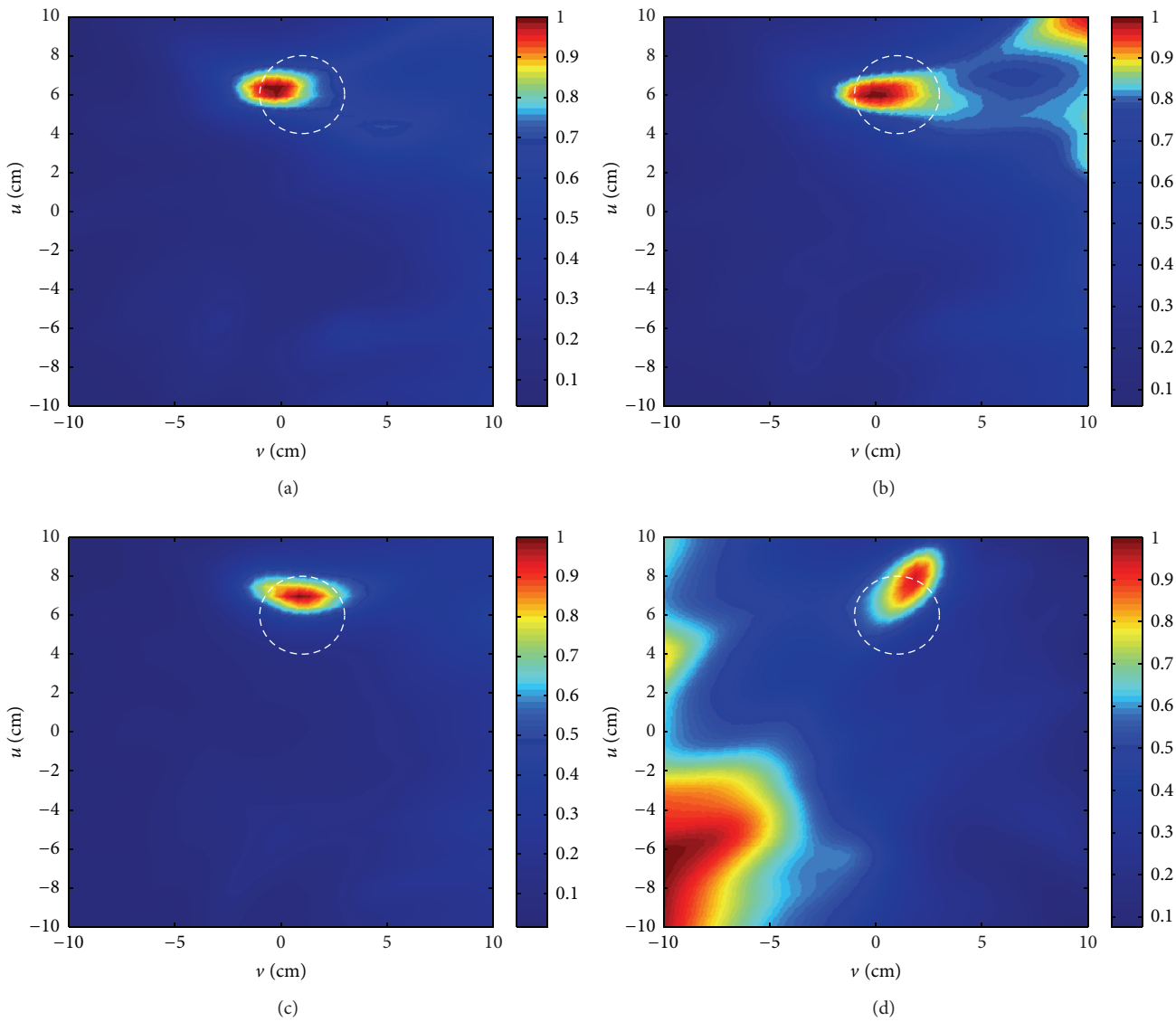

Figure 7: Reconstructions obtained for the air filled scatterer by using (a) LSM, (b) FM when the transmitting and receiving antennas are located on $90^\circ < \theta < 270^\circ$. (c) LSM, (d) FM when the transmitting and receiving antennas are located on $90^\circ < \theta < 270^\circ$, $r = 17$ cm, and $-90^\circ < \theta < 90^\circ$, $r = 17$ cm, respectively.

Conflict of Interests

The authors declare that there is no conflict of interests regarding the publication of this paper.

Acknowledgment

This work is supported by the Scientific and Research Council of Turkey (TUBITAK) under the Project no. 113E977.

References

[1] E. C. Fear, P. M. Meaney, and M. A. Stuchly, "Microwaves for breast cancer detection?" *IEEE Potentials*, vol. 22, no. 1, pp. 12–18, 2003.

[2] E. J. Bond, X. Li, S. C. Hagness, and B. D. van Veen, "Microwave imaging via space-time beamforming for early detection of breast cancer," *IEEE Transactions on Antennas and Propagation*, vol. 51, no. 8, pp. 1690–1705, 2003.

[3] O. Güren, M. Çayören, L. T. Ergene, and I. Akduman, "Surface impedance based microwave imaging method for breast cancer screening: contrast-enhanced scenario," *Physics in Medicine and Biology*, vol. 59, no. 19, pp. 5725–5739, 2014.

[4] I. Catapano, L. Crocco, M. D'Urso, and T. Isernia, "A novel effective model for solving 3-D nonlinear inverse scattering problems in lossy scenarios," *IEEE Geoscience and Remote Sensing Letters*, vol. 3, no. 3, pp. 302–306, 2006.

[5] I. Catapano, L. Crocco, and T. Isernia, "Improved sampling methods for shape reconstruction of 3-D buried targets," *IEEE Transactions on Geoscience and Remote Sensing*, vol. 46, no. 10, pp. 3265–3273, 2008.

[6] Ö. Özdemir and H. Haddar, "Preprocessing the reciprocity gap sampling method in buried-object imaging experiments," *IEEE Geoscience and Remote Sensing Letters*, vol. 7, no. 4, pp. 756–760, 2010.

[7] I. Catapano, F. Soldovieri, and L. Crocco, "On the feasibility of the linear sampling method for 3D GPR surveys," *Progress in Electromagnetics Research*, vol. 118, pp. 185–203, 2011.

[8] T. U. Gürbuz, B. Aslanyürek, E. P. Karabulut, and I. Akduman, "An efficient nonlinear imaging approach for dielectric objects buried under a rough surface," *IEEE Transactions on Geoscience and Remote Sensing*, vol. 52, no. 5, pp. 3013–3022, 2014.

[9] M. N. Akıncı and M. Çayören, "Microwave subsurface imaging of buried objects under a rough air-soil interface," *Remote Sensing Letters*, vol. 5, no. 8, pp. 703–712, 2014.

[10] W. C. Chew and Y. M. Wang, "Reconstruction of two-dimensional permittivity distribution using the distorted born iterative method," *IEEE Transactions on Medical Imaging*, vol. 9, no. 2, pp. 218–225, 1990.

[11] A. Abubakar and P. M. van den Berg, "The contrast source inversion method for location and shape reconstructions," *Inverse Problems*, vol. 18, no. 2, pp. 495–510, 2002.

[12] R. Potthast, "A survey on sampling and probe methods for inverse problems," *Inverse Problems*, vol. 22, no. 2, pp. R1–R47, 2006.

[13] M. Pastorino, *Microwave Imaging*, John Wiley & Sons, New York, NY, USA, 2010.

[14] F. Cakoni and D. Colton, *A Qualitative Approach to Inverse Scattering Theory*, Springer, Berlin, Germany, 2013.

[15] D. Colton and P. Monk, "A linear sampling method for the detection of leukemia using microwaves," *SIAM Journal on Applied Mathematics*, vol. 58, no. 3, pp. 926–941, 1998.

[16] D. Colton and P. Monk, "A linear sampling method for the detection of leukemia using microwaves II," *SIAM Journal on Applied Mathematics*, vol. 60, no. 1, pp. 241–255, 1999.

[17] G. Bozza, M. Brignone, and M. Pastorino, "Application of the no-sampling linear sampling method to breast cancer detection," *IEEE Transactions on Biomedical Engineering*, vol. 57, no. 10, pp. 2525–2534, 2010.

[18] L. Crocco, I. Catapano, L. di Donato, and T. Isernia, "The linear sampling method as a way to quantitative inverse scattering," *IEEE Transactions on Antennas and Propagation*, vol. 60, no. 4, pp. 1844–1853, 2012.

[19] R. Scapaticci, L. di Donato, I. Catapano, and L. Crocco, "A feasibility study on microwave imaging for brain stroke monitoring," *Progress in Electromagnetics Research B*, vol. 40, pp. 305–324, 2012.

[20] L. di Donato, M. T. Bevacqua, L. Crocco, and T. Isernia, "Inverse scattering via virtual experiments and contrast source regularization," *IEEE Transactions on Antennas and Propagation*, vol. 63, no. 4, pp. 1669–1677, 2015.

[21] L. Di Donato and L. Crocco, "Model-based quantitative cross-borehole gpr imaging via virtual experiments," *IEEE Transactions on Geoscience and Remote Sensing*, vol. 53, no. 8, pp. 4178–4185, 2015.

[22] F. Cakoni, D. Colton, and P. Monk, *The Linear Sampling Method in Inverse Electromagnetic Scattering*, vol. 80 of *CBMS-NSF Regional Conference Series in Applied Mathematics*, SIAM, 2011.

[23] A. Kirsch and N. Grinberg, *The Factorization Method for Inverse Problems*, Oxford University Press, New York, NY, USA, 2007.

[24] T. P. Montoya, "Land mine detection using a ground-penetrating radar based on resistively loaded Vee dipoles," *IEEE Transactions on Antennas and Propagation*, vol. 47, no. 12, pp. 1795–1806, 1999.

[25] M. Sato, Y. Hamada, X. Feng, F. Kong, Z. Zeng, and G. Fang, "GPR using an array antenna for landmine detection," *Near Surface Geophysics*, vol. 2, no. 1, pp. 7–13, 2004.

[26] A. A. Vertiy, S. P. Gavrilov, V. N. Stepanyuk, and I. V. Voynovskyy, "Through-wall and wall microwave tomography imaging," in *Proceedings of the IEEE Antennas and Propagation Society International Symposium*, vol. 3, pp. 3087–3090, IEEE, June 2004.

[27] I. Catapano and L. Crocco, "A qualitative inverse scattering method for through-the-wall imaging," *IEEE Geoscience and Remote Sensing Letters*, vol. 7, no. 4, pp. 685–689, 2010.

[28] W. C. Chew, *Waves and Fields in Inhomogeneous Media*, vol. 522, IEEE Press, New York, NY, USA, 1995.

[29] D. Colton, H. Haddar, and M. Piana, "The linear sampling method in inverse electromagnetic scattering theory," *Inverse Problems*, vol. 19, no. 6, pp. S105–S137, 2003.

[30] I. Catapano, L. Crocco, and T. Isernia, "On simple methods for shape reconstruction of unknown scatterers," *IEEE Transactions on Antennas and Propagation*, vol. 55, no. 5, pp. 1431–1436, 2007.

[31] M. N. Akinci, T. Caglayan, S. Ozgur et al., "Qualitative microwave imaging with scattering parameters measurements," *IEEE Transactions on Microwave Theory and Techniques*. In press.

[32] I. Catapano, L. Crocco, M. D' Urso, and T. Isernia, "3D microwave imaging via preliminary support reconstruction: testing on the Fresnel 2008 database," *Inverse Problems*, vol. 25, no. 2, Article ID 024002, 23 pages, 2009.

[33] A. Kirsch, "Factorization of the far-field operator for the inhomogeneous medium case and an application in inverse scattering theory," *Inverse Problems*, vol. 15, no. 2, pp. 413–429, 1999.

[34] A. Kirsch, "The factorization method for Maxwell's equations," *Inverse Problems*, vol. 20, no. 6, pp. S117–S134, 2004.

[35] A. Lechleiter, "A regularization technique for the factorization method," *Inverse Problems*, vol. 22, no. 5, pp. 1605–1625, 2006.

[36] F. S. Bazán, J. B. Francisco, K. H. Leem, and G. Pelekanos, "A maximum product criterion as a Tikhonov parameter choice rule for Kirsch's factorization method," *Journal of Computational and Applied Mathematics*, vol. 236, no. 17, pp. 4264–4275, 2012.

[37] E. Gazit, "Improved design of the vivaldi antenna," *IEE Proceedings H: Microwaves, Antennas and Propagation*, vol. 135, no. 2, pp. 89–92, 1988.

[38] M. Chiappe and G. L. Gragnani, "Vivaldi antennas for microwave imaging: theoretical analysis and design considerations," *IEEE Transactions on Instrumentation and Measurement*, vol. 55, no. 6, pp. 1885–1891, 2006.

[39] B. Zhou, H. Li, X. Y. Zou, and T.-J. Cui, "Broadband and high-gain planar vivaldi antennas based on inhomogeneous anisotropic zero-index metamaterials," *Progress in Electromagnetics Research*, vol. 120, pp. 235–247, 2011.

[40] M. Çayören, M. Abbak, and İ. Akduman, "Microwave breast phantom measurements with a cavity-backed Vivaldi antenna," *IET Microwaves, Antennas & Propagation*, vol. 8, no. 13, pp. 1127–1133, 2014.

[41] O. M. Bucci and T. Isernia, "Electromagnetic inverse scattering: retrievable information and measurement strategies," *Radio Science*, vol. 32, no. 6, pp. 2123–2137, 1997.

[42] J.-M. Geffrin, C. Eyraud, A. Litman, and P. Sabouroux, "Optimization of a bistatic microwave scattering measurement setup:

from high to low scattering targets," *Radio Science*, vol. 44, no. 2, 2009.

[43] C. A. Balanis, *Advanced Engineering Electromagnetics*, vol. 20, John Wiley & Sons, New York, NY, USA, 1989.

[44] B. B. Guzina, F. Cakoni, and C. Bellis, "On the multi-frequency obstacle reconstruction via the linear sampling method," *Inverse Problems*, vol. 26, no. 12, Article ID 125005, 29 pages, 2010.

[45] H. Gan and W. C. Chew, "A discrete BCG-FFT algorithm for solving 3D inhomogeneous scatterer problems," *Journal of Electromagnetic Waves and Applications*, vol. 9, no. 10, pp. 1339–1357, 1995.

[46] N. Wagner, K. Emmerich, F. Bonitz, and K. Kupfer, "Experimental investigations on the frequency- and temperature-dependent dielectric material properties of soil," *IEEE Transactions on Geoscience and Remote Sensing*, vol. 49, no. 7, pp. 2518–2530, 2011.

[47] P. P. Bobrov, A. V. Repin, and O. V. Rodionova, "Wideband frequency domain method of soil dielectric property measurements," *IEEE Transactions on Geoscience and Remote Sensing*, vol. 53, no. 5, pp. 2366–2372, 2015.

[48] W. J. Ellison, K. Lamkaouchi, and J.-M. Moreau, "Water: a dielectric reference," *Journal of Molecular Liquids*, vol. 68, no. 2-3, pp. 171–279, 1996.

[49] B. Aslanyurek, H. Sahinturk, and M. Cayoren, "Microwave imaging of a slightly varying 2-D conducting object through generalized impedance boundary conditions," *IEEE Geoscience and Remote Sensing Letters*, vol. 11, no. 11, pp. 1851–1855, 2014.

[50] D. Colton, P. Monk, and F. Cakoni, "Applications of electromagnetic waves to problems in nondestructive testing and target identification," DTIC Document, Technical Report, 2014.

[51] M. Pastorino, A. Randazzo, A. Fedeli et al., "A microwave tomographic system for wood characterization in the forest products industry," *Wood Material Science & Engineering*, vol. 10, no. 1, pp. 75–85, 2015.